THE ASTROPHYSICAL JOURNAL, 654:544–550, 2007 January 1

MOST[1] DETECTS g-MODES IN THE LATE-TYPE Be STAR β CANIS MINORIS (B8 Ve)

H. SAIO,[2] C. CAMERON,[3] R. KUSCHNIG,[3] G. A. H. WALKER,[4] J. M. MATTHEWS,[3] J. F. ROWE,[3] U. LEE,[2] D. HUBER,[5] W. W. WEISS,[5] D. B. GUENTHER,[6] A. F. J. MOFFAT,[7] S. M. RUCINSKI,[8] AND D. SASSELOV[9]

Received 2006 July 24; accepted 2006 September 14

ABSTRACT

The *Microvariability and Oscillations of Stars* (*MOST*) satellite has detected low-amplitude light variations ($\Delta m \sim 1$ mmag) in the Be star β CMi (B8 Ve). The observations lasted 41 days and the variations have typical periods $\sim$0.3 days. We demonstrate that the dominant frequencies are consistent with prograde high-order g-modes of $m = -1$ excited by the Fe bump of opacity in an intermediate-mass ($\approx 3.5\ M_\odot$) star with a nearly critical rotation period of 0.38 days. This is the first detection of nonradial g-mode pulsations in a Be star later than B6 leading to the possibility that pulsations are excited in all classical Be stars.

Subject headings: stars: early-type — stars: emission-line, Be — stars: individual (β Canis Minoris) — stars: oscillations — stars: rotation

Online material: color figure

1. INTRODUCTION

Be stars are non-supergiant, rapid rotators, which at times show emission in the Balmer and certain metallic lines. They are often called "classical Be stars" to distinguish them from other emission line stars such as Herbig Ae/Be stars and Algol systems (see Porter & Rivinius 2003 for a recent review on Be stars). The line emission is assumed to arise in a geometrically thin disk consisting of matter ejected from the central star. Such circumstellar disks have actually been imaged by long-baseline interferometry for several Be stars, including β CMi (e.g., Tycner et al. 2005). Our target star, β CMi (HD 58715, HR 2845), is a bright but "quiet" late-type Be star (B8 Ve; $V = 2.886$, $B - V = -0.072$); no photometric variations were found by Pavlovski et al. (1997). The star shows only gradual and small long-term variations in Hα emission (e.g., Hanuschik et al. 1996) arising from a relatively small disk of $\sim$3 stellar radii (e.g., Tycner et al. 2005).

Other Be stars, particularly of early type, often show short-term photometric variations of less than a few days. The causes of these variations are assumed to be pulsation and rotational modulation (see Porter & Rivinius 2003 for a review). Many early-type Be stars exhibit line-profile variations indicating the presence of nonradial pulsations (e.g., Rivinius et al. 2003). Multiperiodic photometric variations are also the signature of nonradial pulsations such as those found recently by *MOST* for ζ Oph (O9.5 Ve; Walker et al. 2005a) and HD 163868 (B5 Ve; Walker et al. 2005b). Until now, there has been no clear indication of pulsations for late-type Be stars. Baade (1989) searched for, but failed to detect any line-profile variations in B8 to B9.5 stars. There were very small photometric variations in a few late-type Be stars, but these were judged to be monoperiodic (e.g., μ Pic B9 Ve, Balona et al. 1992; ζ Crv B8 Vne, Barrera et al. 1991) and attributed to rotational modulation.

It is of critical importance to know if nonradial pulsations are excited even in late-type Be stars because it would indicate that all Be stars may have nonradial pulsations that could play a critical role in mass ejection. Excitation of g-modes in late-type Be stars is likely because the cool boundary of the distribution of Be stars on the HR diagram (Zorec et al. 2005) roughly coincides with the cool boundary of the slowly pulsating B (SPB) stars (Pamyatnykh 1999), and because prograde g-modes can be excited even in a rapidly rotating star (Walker et al. 2005b). With this motivation we observed β CMi with *MOST* and indeed discovered multiperiodic light variations, albeit of low amplitude.

2. THE *MOST* PHOTOMETRY

The *MOST* satellite was launched on 2003 June and the original mission is described by Walker et al. (2003). A 15/17.3 cm Rumak-Maksutov telescope feeds two CCDs, one for tracking and the other for science, through a single, custom, broadband filter (350–700 nm). Starlight from primary science targets ($V \leq 6$) is projected onto the science CCD as a fixed (Fabry) image of the telescope pupil covering about 1500 pixels for high photometric stability and insensitivity to detector flat-field irregularities and the effect of particle irradiation on individual pixels. The experiment was designed to detect photometric variations with periods of minutes at micromagnitude precision and does not rely on comparison stars or flat-fielding for the Fabry photometry. There is no direct connection to any photometric system. Tracking jitter was dramatically reduced by early 2004 to $\sim 1''$, which led to significantly higher precision in the Fabry photometry.

[1] Based on data from the *MOST* satellite, a Canadian Space Agency mission, jointly operated by Dynacon Inc., the University of Toronto Institute of Aerospace Studies, and the University of British Columbia with the assistance of the University of Vienna.

[2] Astronomical Institute, Graduate School of Science, Tohoku University, Sendai, Japan; saio@astr.tohuku.ac.jp, lee@astr.tohoku.ac.jp.
[3] Department of Physics and Astronomy, University of British Columbia, Vancouver, BC, Canada; kuschnig@astro.phys.ubc.ca, matthews@phas.ubc.ca, ccameron@phas.ubc.ca, rowe@phas.ubc.ca.
[4] 1234 Hewlett Place, Victoria, BC, Canada; gordonwa@uvic.ca.
[5] Institut für Astronomie, Universität Wien Türkenschanzstrasse 17, Wien, Austria; huber@astro.univie.ac.at, weiss@astro.univie.ac.at.
[6] Department of Astronomy and Physics, St. Mary's University Halifax, NS, Canada; guenther@ap.stmarys.ca.
[7] Département de physique, Université de Montréal, Montréal, QC, Canada and Observatoire du Mont Mégantic; moffat@astro.umontreal.ca.
[8] Department of Astronomy and Astrophysics, David Dunlap Observatory, University of Toronto, Richmond Hill, ON, Canada; rucinski@astro.utoronto.ca.
[9] Harvard-Smithsonian Center for Astrophysics Cambridge, MA; sasselov@cfa.harvard.edu.

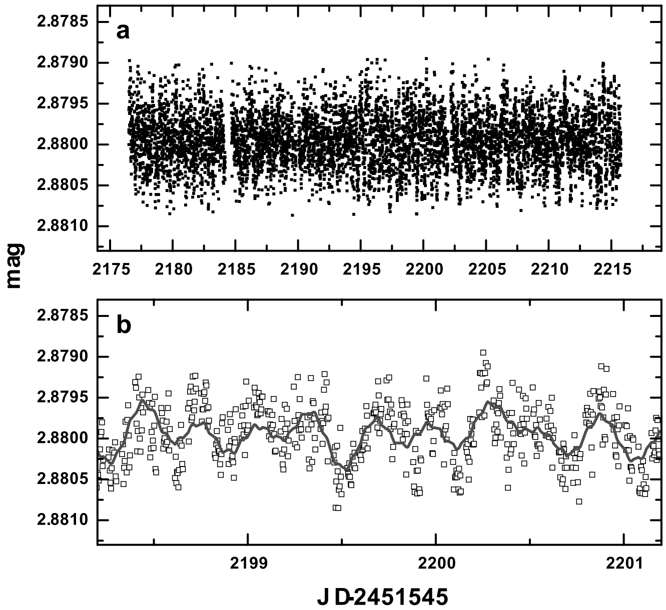

Fig. 1.—(*a*) *MOST* 41 day light curve of β CMi. Each point is a 5 minute mean and the point-to-point rms scatter is 0.070 mmag. (*b*) An expanded 3 day portion of the light curve in (*a*). The solid line is the fit of the 20 highest peaks from the frequency analysis of the full light curve. [*See the electronic edition of the Journal for a color version of this figure.*]

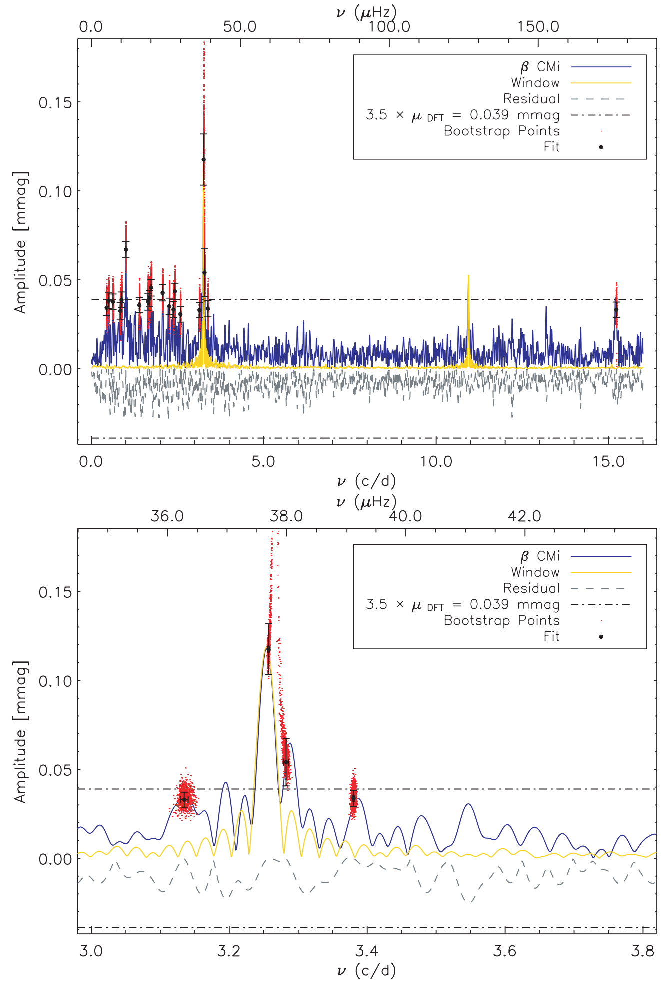

Fig. 2.—*Top*: Fourier amplitude spectrum of the light curve in Fig. 1. The points with bars are frequencies returned by CAPER having the largest amplitudes. The window function is shown for the strongest peak. Residuals after removing the 20 largest peaks are shown at the bottom of the panel (the sign is inverted for better visibility). Small dots indicate the frequency and amplitude obtained at each bootstrap (e.g., Wall & Jenkins 2003), in which the frequency analysis by CAPER was repeated many times for data sets consisting of randomly chosen data points (see Saio et al. 2006 for details). Dash-dotted lines indicate a level of 3.5 × the noise averaged over the spectrum from 0 to 15 cycles day^{-1}. *Bottom*:A zoomed region around the most prominent peak. Note that all identified frequencies are resolved.

The observations received from the satellite were reduced by R. K. Outlying data points generated by poor tracking or cosmic-ray hits were removed. *MOST* suffers from parasitic light, mostly Earthshine, at certain orbital phases, with the amount and phase depending on the stellar coordinates, spacecraft roll, and season of the year. Data are also recorded for Fabry images from seven of the eight lenses adjacent to the target Fabry lens in order to track the stray light background. These background signals were combined in a mean and subtracted from the target photometry. This also corrected for bias, dark, and background signals, and their variations. The reductions basically followed the scheme outlined earlier by Rucinski et al. (2004).

MOST observed β CMi from 2005 December 16 until 2006 January 26 for a total of 41 days. Observing time was split between β CMi and another field such that only 45% of each 101 minute orbit was available for β CMi. In addition to the 45% duty cycle over the 41 days, there was a single ~12 hr gap. Individual exposures were 8 s taken every 20 s (the sampling time). For the final frequency analysis mean magnitudes were calculated from data accumulated every 5 minutes. The rms scatter of the individual 8 s exposures is 0.300 mmag and 0.070 mmag for the 5 minute means.

Figure 1 displays the full 41 day light curve for the 5 minute means with time in heliocentric JD. A 3 day expanded portion of the light curve is shown in the second panel. The solid line in the lower panel is the reconstructed light curve obtained with the most significant peaks in the frequency analysis discussed below. The complete light curve can be downloaded from the *MOST* Public Data Archive .[10]

Figure 2 displays the discrete Fourier transform (DFT) of the *MOST* light curve for β CMi. The frequency analysis was performed by C. C. using his CAPER software (Walker et al. 2005b; Saio et al. 2006). Frequencies with amplitudes $\gtrsim$0.04 mmag (3.5 times the noise level averaged over the spectrum from 0 to 15 cycles day^{-1}) are identified in Figure 2. The plot includes the spectral window function and shows the residual amplitude spectrum after removal of the 20 highest peaks. The peak at 1 cycles day^{-1} is an artifact of the Earth's rotation and the satellite's Sun-synchronous orbit, and their modulation of parasitic light. The peak at 15.2 cycles day^{-1} is an artifact related to *MOST*'s orbital frequency.

There are two dominant features in the DFT, with frequencies of 3.257 ± 0.001 cycles day^{-1} (signal-to-noise ratio [S/N]~8.5) and 3.282 ± 0.004 cycles day^{-1} (S/N ~ 3.5). The spacing between these two frequencies is 0.025 ± 0.004 cycles day^{-1}. The high S/N values for these frequencies and detailed comparison with the background recorded in the *MOST* Fabry field demonstrates that these two signals are intrinsic to β CMi.

There are also nearby frequencies at 3.135 ± 0.006 cycles day^{-1} (S/N ~ 2.9) and 3.380 ± 0.002 cycles day^{-1} (S/N ~ 2.8). However, given their relatively low S/N, we do not consider these to be definitive detections in this data set. There is also evidence for

[10] The *MOST* Public Data Archive is available at http://www.astro.ubc.ca/MOST.

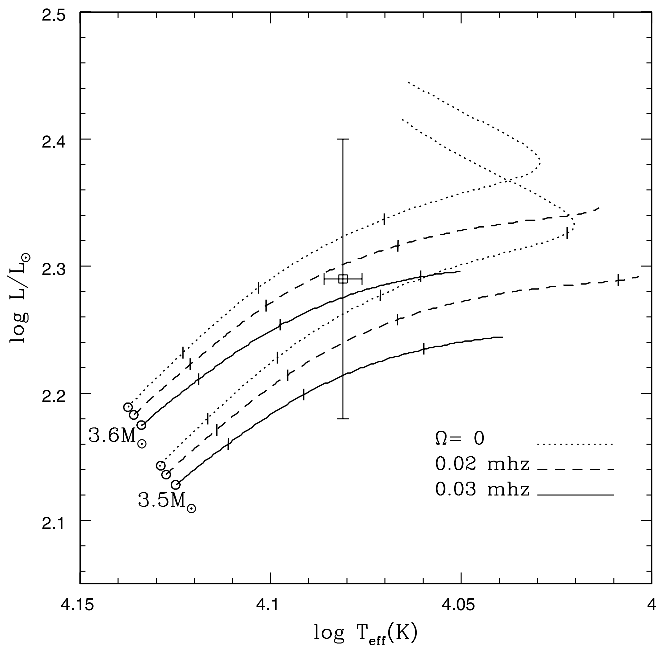

Fig. 3.—Evolutionary tracks of 3.5 and 3.6 $M_\odot$ with various rotation frequencies. Circles indicate positions of zero-age main sequence models. Tic marks along each evolutionary track indicate positions separated by an interval of 5×10^7 yr. The square with error bars indicates the approximate position of β CMi.

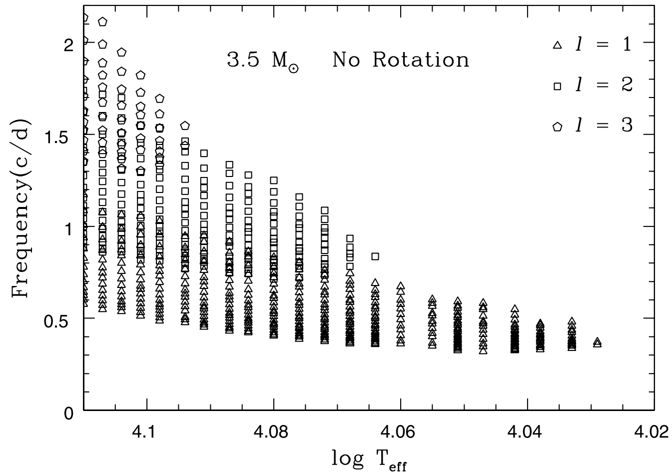

Fig. 4.—Frequencies of g-modes excited in nonrotating models along the 3.5 $M_\odot$ main-sequence evolution. The evolutionary track is shown in Fig. 3.

significant stellar variability at frequencies below 3 cycles day^{-1}, but its origin is unclear.

We have performed the frequency analysis on the data, with the long-term trends both removed and left in the time series. The frequency identifications reported above are unaffected, which is consistent with the very clean spectral window of the *MOST* photometry and the expected lack of power leakage from low to higher frequencies in the Fourier spectrum of these data.

Error bars for the fit parameters are determined by a bootstrap process (e.g., Wall & Jenkins 2003). A large number of trial light curves (10,000 in this case) are generated by randomly sampling the β CMi light curve. The fitting procedure is repeated for each new light curve resulting in a distribution for each fit parameter. The error bars are 1 standard deviation in each of the parameter distributions (see for example Saio et al. 2006). Note that these frequencies are well determined although the amplitudes of the main peaks have moderate uncertainties.

3. MODELS

To understand the cause of the periodic variations detected by *MOST*, we have performed a pulsational stability analysis for rapidly rotating main-sequence star models of 3.5 and 3.6 $M_\odot$, whose evolutionary tracks pass close to the position of β CMi (Fig. 3). The evolutionary models were computed in the same way as in Walker et al. (2005b), and the stability analysis was performed based on the method of Lee & Baraffe (1995). An initial chemical composition of $(X, Z) = (0.70, 0.02)$ is adopted. The opacity was obtained from OPAL tables (Iglesias & Rogers 1996). The centrifugal force is approximately included in the spherical symmetric hydrostatic equilibrium as

$$\frac{dP}{dr} = -g\rho + \frac{2}{3} r\Omega^2, \tag{1}$$

where P is the pressure, r is the distance from the center, g is the local gravitational acceleration, ρ is the matter density, and Ω is the angular frequency of rotation. The rotation frequency is assumed to be constant throughout the stellar interior and evolution. Evolutionary tracks calculated with rotation frequencies of 0.02 mHz (1.73 cycles day^{-1}) and 0.03 mHz (2.59 cycles day^{-1}) are shown in Figure 3. These tracks stop where the centrifugal force exceeds the gravitational force in equation (1) at the stellar surface. A track not including rotational effects has also been calculated and is also shown in Figure 3.

Figure 3 also shows an approximate position of β CMi with error bars, which is estimated as follows. Zorec et al. (2005) obtained ($\log T_{\rm eff}$, $\log g$) = (4.070, 3.88) for β CMi as apparent parameters and converted them to mean values ($\log \overline{T_{\rm eff}}$, $\log \overline{g}$) = (4.081, 3.94) averaged over the whole stellar surface. These parameters yield $\log L/L_\odot = 2.33$. On the other hand, Fabregat & Reglero (1990) obtained an absolute magnitude of $M_v = 0.01$ from the data of $uvby\beta$ photometry corrected for circumstellar emission. Combining this value with a bolometric correction for B8 V of -0.7 (Flower 1977) yields $\log L/L_\odot = 2.18$. Furthermore, combining Fabregat & Reglero's V magnitude of 3.02 (corrected for circumstellar emission) with the *Hipparcos* parallax (Perryman et al. 1997) and the above bolometric correction, we obtain $\log L/L_\odot = 2.41$. From these estimates we have adopted $\log L/L_\odot = 2.29 \pm 0.11$ for the luminosity of β CMi. For the effective temperature, Flower (1977) gives $\log T_{\rm eff} = 4.086$ for the spectral type B8 V. Combining this value and Zorec et al.'s value, we have adopted $\log T_{\rm eff} = 4.081 \pm 0.005$.

β CMi is located close to the cool edge of the SPB instability region of the HR diagram (Pamyatnykh 1999). Our models confirm this observation (see Fig. 4). Along our evolutionary tracks without rotation the cooler boundary of the instability region appears at $\log T_{\rm eff} \approx 4.03$ for $l = 1$, $\approx$4.06 for $l = 2$, and $\approx$4.09 for $l = 3$. The excited modes in our 3.5 $M_\odot$, nonrotating models are high-order g-modes excited by the Fe opacity bump (Gautschy & Saio 1993; Dziembowski et al. 1993).

Since β CMi is a rapid rotator, we have to include the rotation effects in the stability analysis of g-modes. Nonradial pulsations of a rapidly rotating star cannot be represented by a single spherical harmonic and coupled with toroidal velocity fields. In our analysis the angular dependence of pulsation amplitude is expanded using eight spherical harmonics $Y_{l_j}^m$ for a given azimuthal order m ($Y_{l'_j}^m$ for toroidal velocity field), where $l_j = |m| + 2j$ ($l'_j = l_j + 1$) for even modes and $l_j = |m| + 2j + 1$ ($l'_j = l_j - 1$) for odd modes with $j = 0, 1, \ldots, 7$ (see, e.g., Unno et al. [1989] for general discussions on nonradial pulsations of rotating stars).

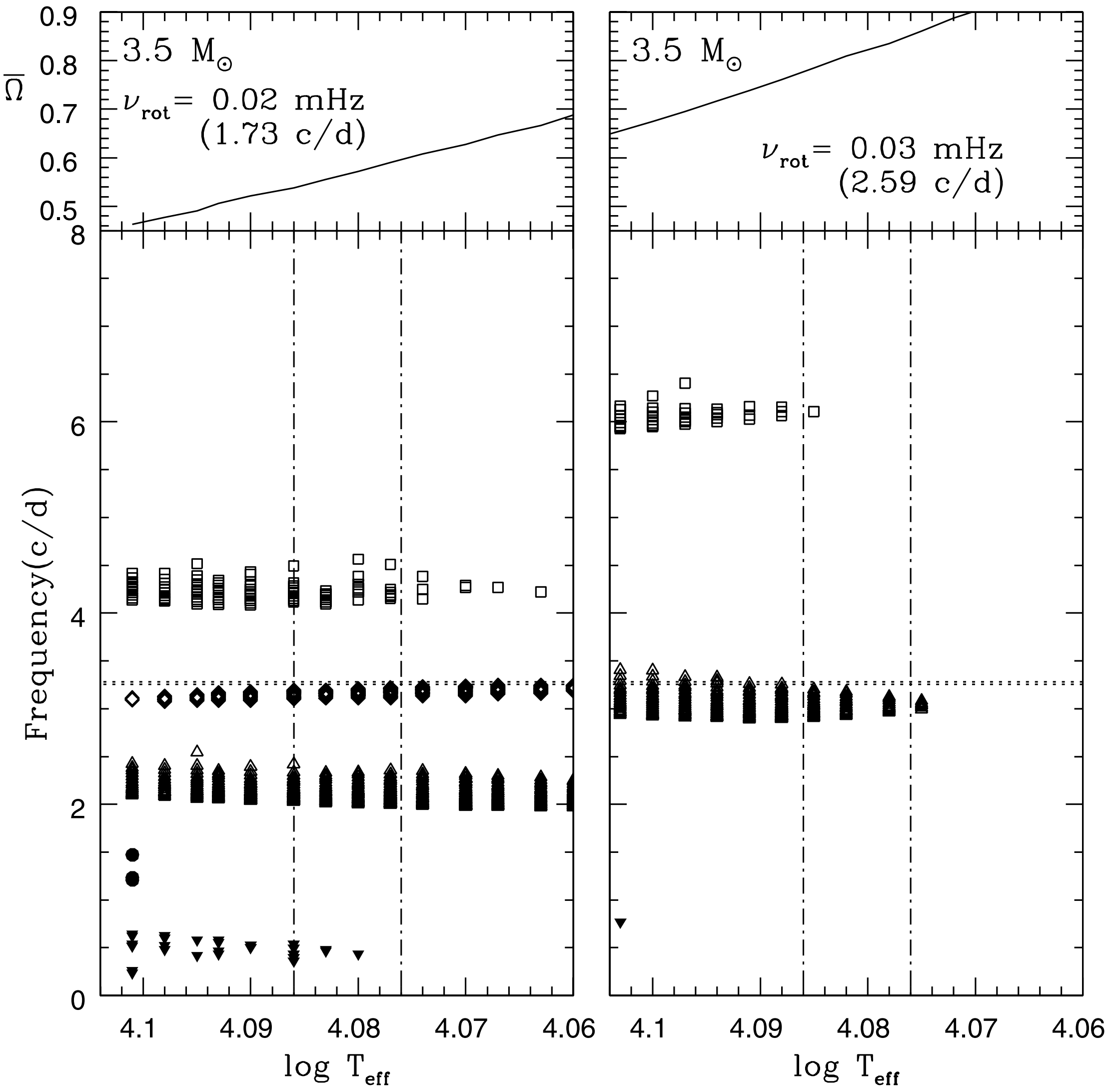

Fig. 5.—Frequencies in the observer's frame of excited pulsation modes (*bottom panels*) and the angular velocity of rotation normalized by $(GM/R^3)^{1/2}$ (*top panels*) as functions of effective temperature. Horizontal dotted lines indicate observed frequencies 3.257 and 3.282 cycles day^{-1} for β CMi. Vertical dash-dotted lines indicate the estimated range for the effective temperature of β CMi. Rotational frequencies are assumed to be 0.02 mHz (*left*) and 0.03 mHz (*right*) through the main-sequence evolution. Symbols indicate type of modes: filled circles for $m = 0, \ell = 1$; triangles) for $m = -1, \ell = 1$; squares for $m = -2, \ell = 2$; inverted triangles for $m = 1, \ell = 2$; and diamonds for $m = 2, \ell = 2$. Only r-modes are excited among retrograde modes ($m > 0$). Other excited modes are sectoral prograde g-modes. (A few axisymmetric g-modes are also excited in the hottest models.)

We adopt the convention that a *negative m* represents a *prograde* mode (in the corotating frame) with respect to the stellar rotation. Even (odd) modes are symmetric (antisymmetric) with respect to the equatorial plane. We designate the angular-dependence type of a mode by a set of (m, ℓ), in which ℓ is defined as the l_j value of the largest-amplitude component.

Figure 5 shows frequencies (in the observer's frame) of low surface order ($|m| \leq 2$ and $\ell \leq 2$) modes excited in evolutionary models of 3.5 $M_\odot$ rotating at frequencies of 0.02 mHz and 0.03 mHz as a function of the effective temperature. Comparing this figure with Figure 4, we find that the cooler boundary of instability is bluer than in the nonrotating case. Fewer modes are excited in more rapidly rotating models. This implies rapid rotation tends to stabilize g-mode pulsations.

The pulsation frequency in the observer's frame is given as

$$|\nu(\mathrm{crot}) - m\nu_{\mathrm{rot}}|,$$

where ν(crot) is the pulsation frequency in the frame corotating at frequency ν_{rot}. Therefore, pulsation frequencies in the observer's frame for high-order g-modes and r-modes (for which $\nu(\mathrm{crot}) \ll |m|\nu_{\mathrm{rot}}$) tend to group depending on the m value just as seen in Figure 5. All the excited prograde modes ($m < 0$) seen in Figure 5 are sectoral ($\ell = |m|$) g-modes, while all the excited retrograde ($m > 0$) modes are r-modes (in which toroidal motion is dominant) in those rapidly rotating models. No retrograde g-modes are excited in this figure. We note that, as shown in the Appendix, the stability of pulsation modes differs considerably if we use the so-called traditional approximation in which the horizontal component of the angular velocity of rotation is neglected.

Under the assumption of $\nu_{\mathrm{rot}} \approx 0.02$ mHz (1.73 cycles day^{-1}), the periodic light variations of β CMi are approximately reproduced by r-modes of $(m, \ell) = (2, 2)$. On the other hand, the observed variations are identified as sectoral prograde g-modes of $(m, \ell) = (-1, 1)$ if we assume $\nu_{\mathrm{rot}} \approx 0.03$ mHz (2.59 cycles day^{-1}). In the former case another three groups of frequencies are expected to be observed in the estimated $\log T_{\mathrm{eff}}$ range of β CMi, while in the latter case only one group of frequencies should be observed (Fig. 5). Since *MOST* has detected only one group of frequencies around 3.26 cycles day^{-1} in β CMi (§ 2), we conclude that a model rotating at $\nu_{\rm rot} \approx 0.03$ mHz (2.59 cycles day^{-1}) is more appropriate.[11] For this rotation rate pulsations excited at log $T_{\rm eff} = 4.083$ are prograde sectoral high-radial order (19th–33rd) g-modes. The frequencies in the corotating frame range over $0.586 \gtrsim \nu(\text{crot}) \gtrsim 0.334$ cycles day^{-1}. Frequency spacings between two adjacent modes lie in a range from 0.035 to 0.009 cycles day^{-1}. Since the frequency resolution expected from the data is approximately (41 days)$^{-1} = 0.024$ cycles day^{-1}, only a few frequencies are expected to be resolved just as the DFT indicates (Fig. 2).

The top panels of Figure 5 show the rotation angular frequency $\overline{\Omega}$ normalized by the Keplerian frequency $(GM/R^3)^{1/2}$. For a given $\nu_{\rm rot}$, $\overline{\Omega}$ increases as the model evolves because the stellar radius R increases. Since the equatorial radius is larger than the mean radius, the rotation velocity becomes critical at the equator with $\overline{\Omega} < 1$; probably at $\overline{\Omega} \sim 0.8$. Figure 5 indicates that 3.5 $M_\odot$ models with $\nu_{\rm rot} = 0.03$ mHz rotate nearly critically at the effective temperature of β CMi. (For 3.6 $M_\odot$ models with $\nu_{\rm rot} = 0.03$ mHz, $\overline{\Omega} > 0.8$, not appropriate for β CMi.) This supports Townsend et al.'s (2004) claim that classical Be stars may be rotating much closer to their critical velocities than is generally supposed. It is also consistent with the recent statistical property found by Cranmer (2005) that the coolest Be stars rotate nearly critically.

4. DISCUSSION

We have found nonradial g-mode pulsations excited in the late-type Be star β CMi (B8 Ve). This confirms that β CMi belongs to the new class of SPBe stars, like HD 163868 (Walker et al. 2005b). We have identified pulsation modes as prograde sectoral g-modes of $m = -1$, based on the comparison between the observed frequencies and theoretical ones excited by the Fe bump of opacity in rapidly rotating models. The fact that only one group of frequencies is detected by *MOST* is consistent with our prediction of the pulsational stability if β CMi rotates nearly critically. This supports the recent claims (Townsend et al. 2004; Cranmer 2005) that classical Be stars rotate more rapidly than previously thought (70%–80% of the critical rate; e.g., Porter 1996; Chauville et al. 2001). The observed amplitudes are small ($\lesssim$1 mmag). Since β CMi lies close to the red edge of the instability region on the HR diagram, the pulsational instability is not strong and hence the pulsation amplitudes are expected to be small.

Our discovery of nonradial pulsations in β CMi suggests the possibility that nonradial pulsations are involved in all rapidly rotating Be stars. In some early-type Be stars mass ejections are observed to occur at certain pulsation phases (e.g., μ Cen, Porter & Rivinius 2003) suggesting that pulsations trigger mass ejections. It is tempting to speculate that nonradial pulsations may play a crucial role in mass ejection in all Be stars. Osaki (1986) argued that prograde nonradial pulsations can transport angular momentum toward the surface and spin up the equatorial region critically, leading to a mass ejection. Owocki (2005) showed numerically that introducing velocity variations corresponding to a prograde ($m = -2$) nonradial pulsation in a nearly critically rotating stellar atmosphere actually yields a circumstellar Keplerian disk.

Our findings in this paper and Walker et al. (2005b) that *prograde* sectoral g-modes are selectively excited in rapidly rotating Be stars, support the above scenario for mass ejection. Line profile variation (LPV) analyses for early-type Be stars, however, tend to indicate the presence of retrograde modes (Rivinius et al. 2003) rather than prograde modes, contrary to our model findings.

Rivinius et al. (1998) obtained four periods around 0.503 days and two periods around 0.28 days from LPVs in μ Cen, one of the best studied and most active Be stars. (These LPVs of μ Cen were modeled as retrograde [$m = 2$, and 3] modes by Rivinius et al. [2001].) Frequency spacings among each group are about 0.034 cycles day^{-1} or less, which are comparable with the frequency difference 0.025 cycles day^{-1} between the two main frequencies of β CMi (§ 2) and with typical frequency spacings $\sim$0.03 cycles day^{-1} of HD 163868 (Walker et al. 2005b). These frequency spacings are comparable with those of g-modes, although they are close to the limit of the frequency resolution. Longer observations by *MOST* or *COROT* would make g-mode seismology of SPBe stars possible. Also, simultaneous photometric and spectroscopic observations of μ Cen and other Be stars showing conspicuous LPVs and mass-ejection events would be important to understand the connection between nonradial pulsations and mass ejections in Be stars.

We thank Thomas Rivinius, the referee of this paper, for his thoughtful comments. This research has made use of the SIMBAD database, operated at CDS, Strasbourg, France. The Natural Sciences and Engineering Research Council of Canada supports the research of C. C., D. B. G., J. M. M., A. F. J. M., J. F. R., S. M. R., G. A. H. W. A. F. J. M. is also supported by FQRNT (Québec). R. K. is supported by the Canadian Space Agency. W. W. W. is supported by the Austrian Space Agency and the Austrian Science Fund (P17580-N2). H. S. is supported by the 21st Century COE programme of MEXT, Japan.

[11] The slower rotation model might appear to be saved if the low-amplitude frequencies around 2 cycles day^{-1} in Fig. 2 were assigned to g-modes of $(m, \ell) = (-1, 1)$ and the main frequencies around 3.26 cycles day^{-1} to r-modes of $(m, \ell) = (2, 2)$. We consider this highly unlikely, however, since r-modes are not expected to yield luminosity variations much larger than the sectoral g-modes of $(m, \ell) = (-1, 1)$, and because no peaks around 4 cycles day^{-1} corresponding to g-modes of $(m, \ell) = (-2, 2)$ are detected.

APPENDIX

MODE STABILITY UNDER THE TRADITIONAL APPROXIMATION

The pulsation analysis for low-frequency modes of a rapidly rotating star is greatly simplified by the use of the so-called traditional approximation, in which the horizontal component of the angular velocity of rotation ($\Omega \sin\theta$ with θ being the colatitude) is neglected. Under the traditional approximation, eigenfrequencies can be obtained using the same equations as those for nonradial pulsations of nonrotating stars except replacing $\ell(\ell+1)$ with the parameter $\lambda_{\ell,m}$ (see, e.g., Townsend 2005; Lee 2006). The value of $\lambda_{\ell,m}$ deviates from $\ell(\ell+1)$ as the ratio of the rotation to the pulsation frequency (in the corotating frame) increases depending on m and ℓ (e.g., Lee & Saio 1997).

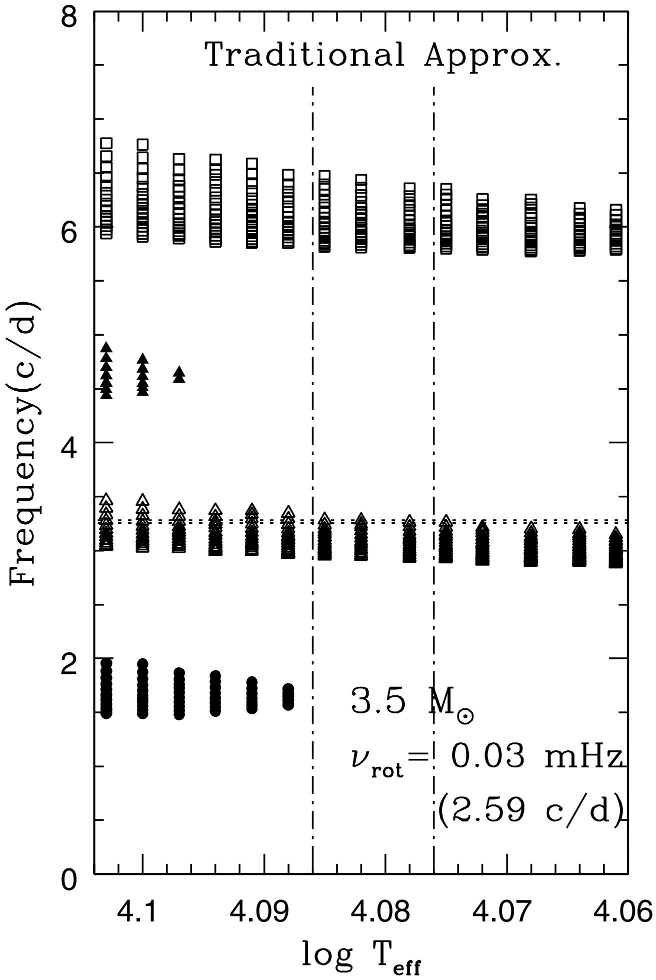

FIG. 6.—Same as the right-bottom panel of Fig. 5, but showing results obtained under the traditional approximation. Filled triangles are for g-modes of $(m, \ell) = (-1, 2)$, and other symbols are the same as in Fig. 5. Compared to Fig. 5 more sectoral g-modes of $m = -1$, and -2 are excited. Tesseral g-modes of $(m, \ell) = (0, 1)$ (around 1.7 cycles day^{-1}) and of $(m, \ell) = (-1, 2)$ (around 4.7 cycles day^{-1}) are excited only under the traditional approximation in these models.

The traditional approximation is justified dynamically for low-frequency pulsations, but it is not clear whether the approximation is reasonable for the nonadiabatic stability analysis. To see the effect, we have performed a stability analysis using the traditional approximation for 3.5 $M_\odot$ models rotating at a frequency of 0.03 mHz. The results are shown in Figure 6. Comparing this figure with Figure 5, we see that under the traditional approximation, larger numbers of prograde sectoral g-modes are excited, and that tesseral g-modes of $(m, \ell) = (0, 1)$ and $(-1, 2)$ are also excited. These tesseral modes are all damped without the traditional approximation in these models. The cause of the difference is attributed to damping due to mode-couplings (Lee 2001), which are absent under the traditional approximation. The damping effect is strongest for retrograde g-modes and tesseral $(\ell > |m|)$ g-modes.

We note that in the models shown in Figure 6, no retrograde g-modes are excited even under the traditional approximation. This is understood as follows. Retrograde g-modes have large values of $\lambda_{\ell,m}$ (Lee & Saio 1997), which correspond to modes of large latitudinal degree ℓ in a nonrotating model. In Figure 4 nonrotating models indicate that the cooler boundary of instability region is hotter for larger ℓ. Therefore, we understand that the temperature range for instability of retrograde g-modes is hotter than that shown in Figure 6.

REFERENCES

Baade, D. 1989, A&A, 222, 200
Balona, L. A., Cuypers, J., & Marang, F. 1992, A&AS, 92, 533
Barrera, L. H., Mennickent, R. E., & Vogt, N. 1991, Ap&SS, 185, 79
Chauville, J., Zorec, J., Ballereau, D., Morrell, N., Cidale, L., & Garcia, A. 2001, A&A, 378, 861
Cranmer, S. R. 2005, ApJ, 634, 585
Dziembowski, W. A., Moskalik, P., & Pamyatnykh, A. A. 1993, MNRAS, 265, 588
Fabregat, J., & Reglero, V. 1990, MNRAS, 247, 407
Flower, P. J. 1977, A&A, 54, 31
Gautschy, A., & Saio, H. 1993, MNRAS, 262, 213
Hanuschik, R. W., Hummel, W., Sutorius, E., Dietle, O., & Thimm, G. 1996, A&AS, 116, 309
Iglesias, C. A., & Rogers, F. J. 1996, ApJ, 464, 943
Lee, U. 2001, ApJ, 557, 311
———. 2006, MNRAS, 365, 677
Lee, U., & Baraffe, I. 1995, A&A, 301, 419
Lee, U., & Saio, H. 1997, ApJ, 491, 839
Osaki, Y. 1986, PASP, 98, 30
Owocki, S. 2005, in ASP Conf. Ser. 337, The Nature and Evolution of Disks around Hot Stars, ed. R. Ignace & K. G. Gayley (San Francisco: ASP), 101
Pamyatnykh, A. A. 1999, Acta Astron., 49, 119
Pavlovski, K., Harmanec, P., Božić, H., Koubský, P., Hadrava, P., Kříž, S., Ružić, Ž., & Štefl, S. 1997, A&AS, 125, 75
Perryman, M. A. C. 1997, The Hipparcos and Tycho Catalogues (ESA SP-1200; Noordwijk: ESA)
Porter, J. M. 1996, MNRAS, 280, L31
Porter, J. M., & Rivinius, T. 2003, PASP, 115, 1153

Rivinius, Th., Baade, D., & Štefl, S. 2003, A&A, 411, 229
Rivinius, Th., Baade, D., Štefl, S., Stahl, O., Wolf, B., & Kaufer, A. 1998, A&A, 336, 177
Rivinius, Th., Baade, D., Štefl, S., Townsend, R. H. D., Stahl, O., Wolf, B., & Kaufer, A. 2001, A&A, 369, 1058
Rucinski, S. M., et al. 2004, PASP, 116, 1093
Saio, H., et al. 2006, ApJ, 650, 1111
Townsend, R. H. D. 2005, MNRAS, 360, 465
Townsend, R. H. D., Owocki, S. P., & Howarth, I. D. 2004, MNRAS, 350, 189
Tycner, C., et al. 2005, ApJ, 624, 359
Unno, W., Osaki, Y., Ando, H., Saio, H., & Shibahashi, H. 1989, Nonradial Oscillations of Stars (Tokyo: Univ. Tokyo Press), chap. 6
Walker, G. A. H., et al. 2003, PASP, 115, 1023
———. 2005a, ApJ, 623, L145
———. 2005b, ApJ, 635, L77
Wall, J. V., & Jenkins, C. R. 2003, Practical Statistics for Astronomers (Cambridge: Cambridge Univ. Press)
Zorec, J., Frémat, Y., & Cidale, L. 2005, A&A, 441, 235